Biomed Eng Lett (2014) 4:95-108
DOI 10.1007/s13534-014-0132-4

REVIEW ARTICLE

Next-generation Flexible Neural and Cardiac Electrode Arrays

Jaemin Kim, Mincheol Lee, Jung Soo Rhim, Pulin Wang, Nanshu Lu and Dae-Hyeong Kim

Received: 13 April 2014 / Revised: 30 May 2014 / Accepted: 10 June 2014

Abstract
The electrical activities of the brain and heart have been recorded and analyzed for diverse clinical and pathological purposes. To construct an implantable system for monitoring the electrical activity effectively, flexible and stretchable electrode arrays that are capable of making conformal contacts on the curvilinear, soft, and dynamic surfaces of the target organs have been extensively researched. Among many strategies, the most representative approach is to fabricate electrode arrays on plastic substrates to achieve more intimate and conformal contact with the target organs. Further optimizations are along with the development of ultrathin and stretchable electronics. Advanced structural modifications, such as thinning the overall profile or applying a mesh-like electrode network, have shown the greatly enhanced conformability and deformability of the device, providing improved signal-to-noise ratios (SNRs). Furthermore, brittle but high-performance silicon transistors have been successfully incorporated in flexible forms by virtue of mechanics-based active electronics designs, enabling the construction of high-density arrays comprising hundreds of multiplexed electrodes that can be individually addressed by only a few external wires. This review summarizes these strategies and describes their strengths and weaknesses, and it suggests possible technologies for next-generation electrode arrays.

Keywords Neural electrode array, Cardiac electrode array, Flexible electrode array, Stretchable electrode array

Jaemin Kim, Mincheol Lee, Jung Soo Rhim, Dae-Hyeong Kim
Center for Nanoparticle Research, Institute for Basic Science (IBS), Seoul 151-742, Republic of Korea

Jaemin Kim†, Mincheol Lee†, Jung Soo Rhim, Dae-Hyeong Kim (✉)
School of Chemical and Biological Engineering, Institute of Chemical Processes, Seoul National University, Seoul 151-742, Republic of Korea
Tel : +82-2-880-1634 / Fax : +82-2-880-7295
E-mail : dkim98@snu.ac.kr

Pulin Wang, Nanshu Lu
Center for Mechanics of Solids, Structures and Materials, Department of Aerospace Engineering and Engineering Mechanics, Texas Materials Institute, University of Texas at Austin, 210 E 24th St., Austin, TX 78712, USA

†J. Kim and M. Lee contributed equally.

INTRODUCTION

Implantable devices for acquiring electrical signals from the heart and the brain have been extensively studied for either short-term clinical applications (electrophysiology and other surgical diagnostic tools) or long-term implant applications (prosthetic devices and human-machine interfaces). Electrophysiological signals measured from the brain have been used for the investigation of abnormal cortical functions, such as the localization of epileptogenic zones [1-4] and to interface the brain with external machines for patients with brain damage [5]. Similarly, electrical signals recorded from the epicardium have been used to characterize arrhythmogenic activities [6]. However, owing to the limitations of conventional electrode array technologies, electrical potentials can be obtained only in the confined area with low resolution, providing only fragmented information of these extremely complex and active organs. This is mainly due to the sparsely distributed electrodes and the large size of an individual electrode. Therefore, studies have strongly focused on developing electrode arrays for electrical signal recording with higher spatial resolution [7-10].

The brain, which comprises roughly a hundred billion neurons, has a complex 3D structure. It has been effectively monitored using penetrating electrodes [11]. These penetrating electrodes are typically made of silicon owing to its well-established micro-machinability and robust mechanical properties, which allow the precise implantation at target locations [12]. Fig. 1a shows the Utah electrode array (UEA, left) and Michigan electrode array (MEA, right), both of which are widely known silicon-based microdevices for

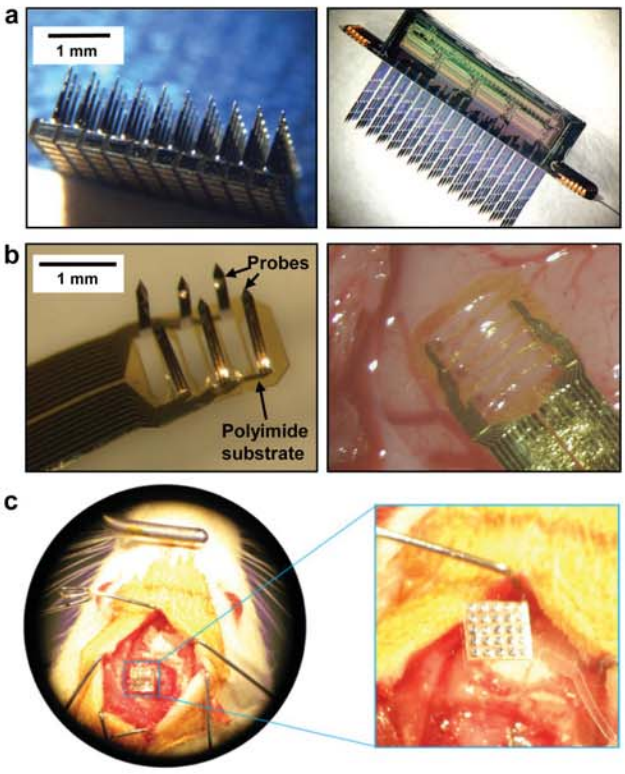

Fig. 1. Several types of penetrating electrode arrays: (a) Silicon-based penetrating electrode array including the Utah electrode array (left) and the Michigan electrode array (right). (left) Reproduced with permission from ref. [20], © 2008, Springer Sceince + Business Media, LLC. (right) Reproduced with permission from ref. [11], © 2007, Nature Publishing Group. (b) Penetrating electrode arrays with flexible shanks (left) and its applied form on rat's brain (right). Reproduced with permission from ref. [19], © 2004, IOP Publishing Ltd. (c) An electrode array of rigid silicon shanks on flexible substrate, implanted on the rat's cerebral cortex. Reproduced with permission from ref. [12], © 2013, IOP Publishing Ltd.

recording or stimulating electrical impulses. Both are thin, rigid arrays of shank-like electrodes that can penetrate the brain tissues and record neuronal signals from deep inside the brain in real time. The UEA receives electrical signals only from the tips and the MEA along the shanks. By penetrating the brain tissues, these electrodes can make intimate contact with target neurons to obtain high-quality signals. However, it is difficult for these electrodes to remain static relative to the neurons owing to the constant mechanical motion of the brain [13] and the extreme elastic mismatch between the rigid silicon ($E_{silicon}$: ~170 GPa) and the soft brain tissue (E_{brain}: ~1 kPa) [14]. This phenomenon may be exacerbated particularly in the case of long-term implantation, which is often accompanied by the inflammation or mechanical damage of the tissue [15-17]. To address this problem, flexible penetrating electrodes that can be synchronously deformed with the movement of the surrounding tissue (Fig. 1b) [18, 19] and rigid penetrating electrodes on a flexible substrate have been reported (Fig. 1c) [20]. However, such penetrating electrodes still have limited lifespans owing to gliosis and encapsulation by fibroblastic tissue, which significantly degrades the signal quality, owing to the penetration-induced causes [21]. To develop reliable, long-term monitoring devices for neural and cardiac signals with minimal tissue damage, therefore, flexible or stretchable surface microelectrode arrays have attracted increasing interest.

In the following, we review various strategies for realizing flexible or stretchable electrode arrays with high spatial resolution for measuring neural and cardiac signals. Different manufacturing technologies, materials, and designs for electrodes and their merits and demerits are described.

CONVENTIONAL ELECTRODE ARRAYS

An electrocorticogram (ECoG) is recorded through electrodes implanted either above or below the dura mater. ECoG measurements have been used by many clinicians and researchers to identify the epileptogenic zone [22, 23] or to build a brain-computer interface (BCI) [24-28, 30]. In keeping with the increasing interest in ECoG signal recording for various applications, several medical instrument companies have commercialized ECoG recording electrode arrays. In these devices, electrodes typically made of biocompatible platinum and stainless steel are placed on flexible substrates made of high-modulus silicone rubber. The distance between the electrodes in commercial ECoG flexible electrode arrays is larger (>3 mm) than that in UEA and MEA (<1 mm) manufactured by microfabrication techniques.

Fig. 2a shows an ECoG electrode array (left) made by AD-Tech Medical Instrument Corporation, one of the leading companies in this area, its applied form on the human brain surface (middle), and signals acquired from it during naming tasks (right). However, such ECoG electrode arrays have a flat continuous silicone sheet that prevents conformal contact with the curved shape of the cortex, which has many wrinkles. To solve this problem, Abel *et al.* modified the electrode array design by cutting it into separate columns to produce a "multi-prong" structure to enhance conformal contact [29]. By using this design, clear event-related spectral perturbations could be obtained from several selected regions. Nonetheless, this device has a low density and a small number of electrodes, which does not provide enough performance in consideration of the complexity and large surface area of the brain, and therefore, data points with limited spatial resolution could be obtained. There is a strong need for devices that would allow for a significantly higher electrode array density to record neural activities for identifying the exact functionality of a selected region of the brain.

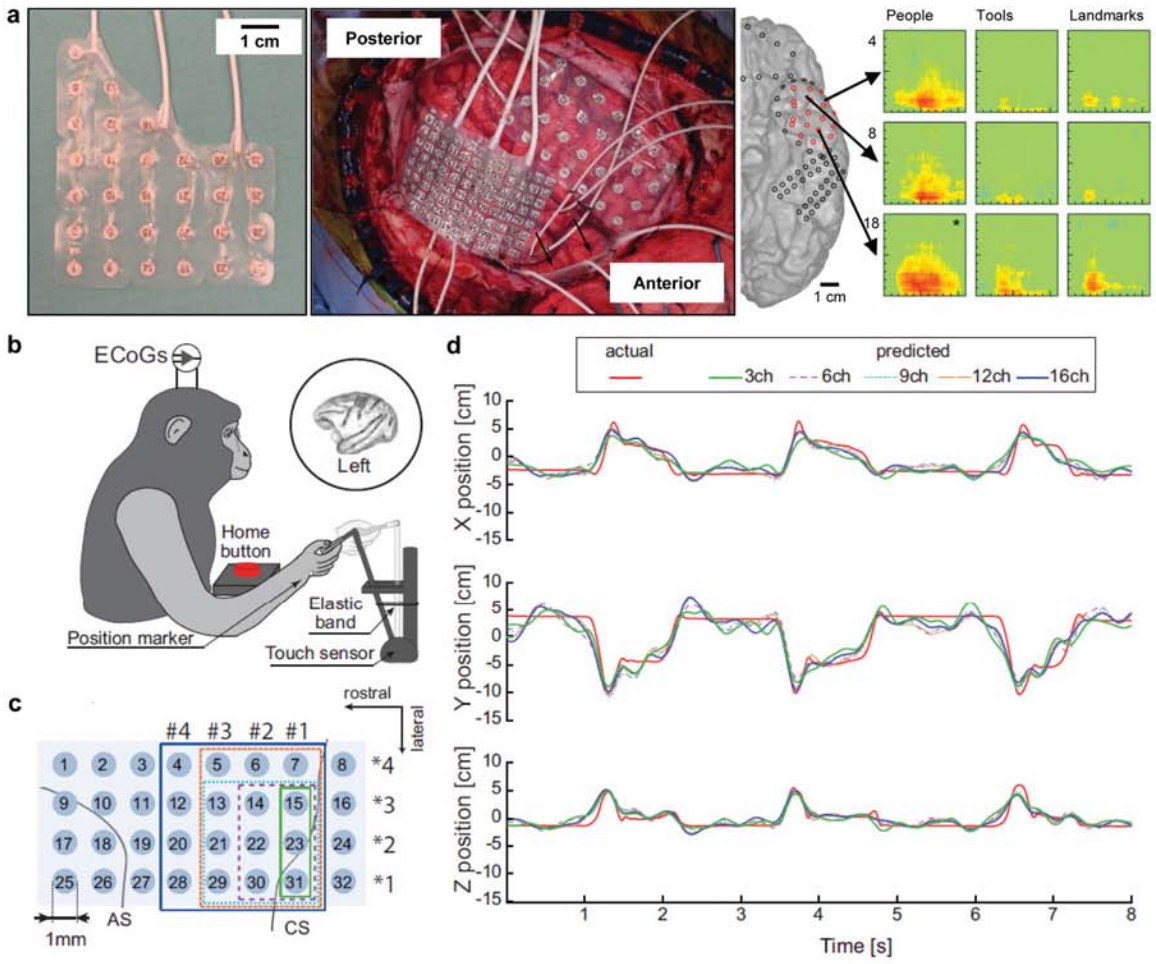

Fig. 2. Commercial flexible electrode arrays and its application: (a) A 30-contact commercial temporal pole grid (left). The electrode array can be placed on the surface of the human brain (middle) to perform spectrotemporal analysis of cortical activity during naming tasks (right). Reproduced with permission from ref. [29], © 2014, Institute of Physics and Engineering in Medicine. (b) Experimental setup for hand trajectory prediction of the monkey using ECoG signal. (c) Group locations of 3 (green solid line), 6 (purple dotted line), 9 (blue dotted line), 12 (brown dotted line) and 16 (blue solid line) electrodes used in decoding. (d) Decoding results with different electrode numbers. The red solid line indicates actual trajectories. The green solid, purple dotted, light blue dotted, brown dotted and blue solid line indicate predicted trajectories using 3, 6, 9, 12, and 16 electrodes, respectively. (b-d) Reproduced from ref. [30], © 2013, Chen *et al.*

Using another commercial ECoG flexible electrode arrays (Unique Medical Co., Ltd., Tokyo, Japan), Chen *et al.* reported that hand trajectories could be predicted using ECoG signals measured on the primary motor cortex of a monkey [30]. Fig. 2b shows the experimental setup to acquire hand movements that can be correlated with the ECoG signals measured from the monkey. The monkey performs the experiments by moving the right hand, such as reaching, grasping, pulling and releasing, in a 3D workspace. Fig. 2c illustrates an arrangement map of the ECoG electrodes. The electrode array was implanted on the gyrus region between the central sulcus and the arcuate sulcus in the primary motor cortex at the left hemisphere. The recorded ECoG signals were further processed based on nine specific frequency bands (1.5~4 Hz, 4~8 Hz, 8~14 Hz, 14~20 Hz, 20~30 Hz, 30~50 Hz, 50~90 Hz, 90~120 Hz, 120~150 Hz). These specific bands are correlated with motor activities, and therefore, the processed ECoG signals could be used in prediction of hand trajectories. Fig. 2d shows the decoding results with different electrode numbers. The prediction performance was improved as the number of electrodes increased up to nine. However, the prediction using more than ten electrodes which cover larger area shows slightly lower performance. The results imply that the ECoG signals from other than effective regions disturb the accurate prediction. In addition, the results also suggest that the higher density of electrodes in effective areas is necessary for the accurate prediction of the limb trajectories using ECoG.

NEW BREAKTHROUGHS IN RECENT ELECTRODE ARRAYS

High-resolution electrode arrays

Microfabrication technologies have been applied to the manufacturing of flexible electrode arrays to reduce the dimension of electrodes and the inter-electrode distance down to the sub-millimeter range for applications requiring high spatial resolutions [31]. For instance, the high spatial resolution of intraocular retinal prosthesis enables direct dictation of artificial vision. To achieve high resolution without a large number of connecting wires, Complementary

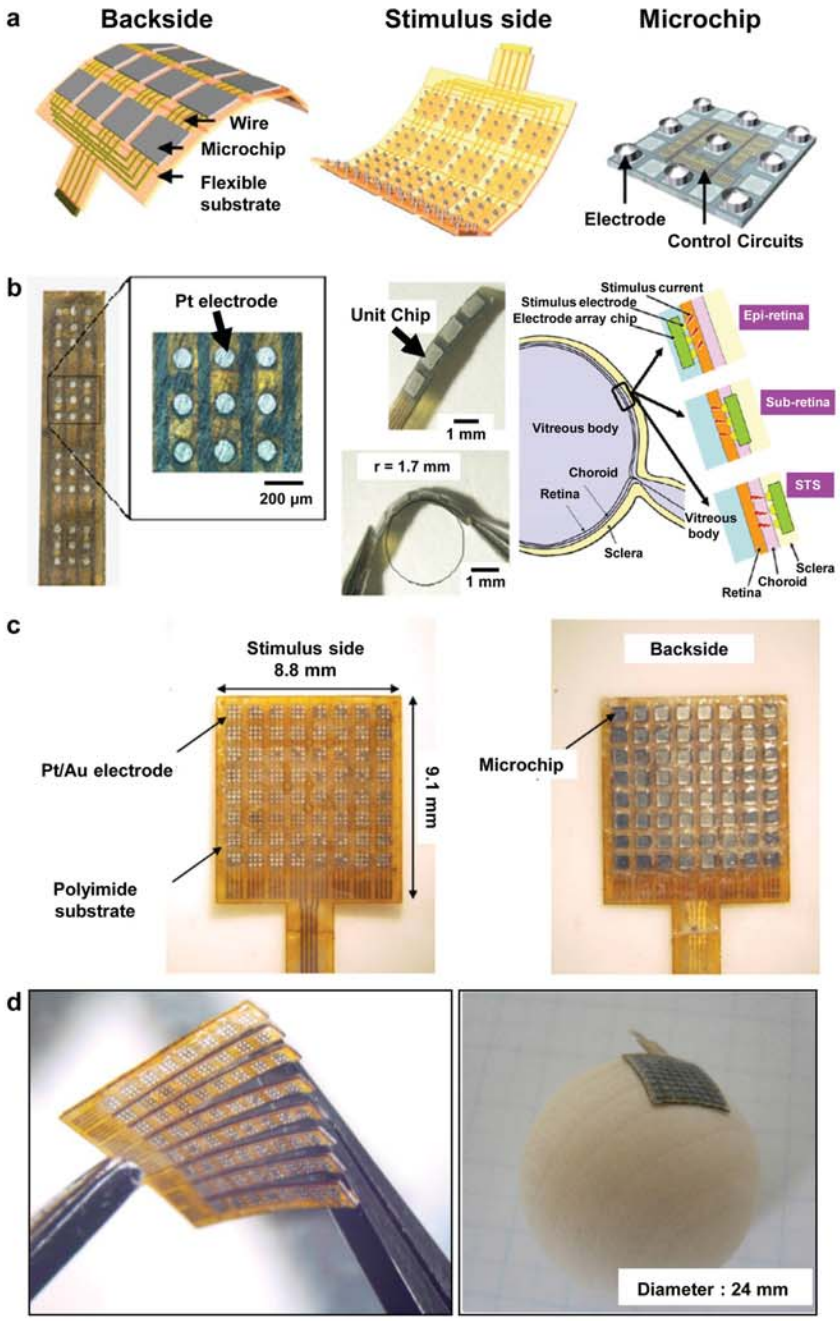

Fig. 3. Flexibility enhancement by using CMOS multichip packaging technology: (a) A schematic structure and components of flexible retinal stimulator. (b) Fabricated retinal stimulator with detailed view of its components (left) and potential implantation sites on retina (right). (a-b) Reproduced with permission from ref. [36], © 2009, Ohta J *et al.* (c) Stimulus side of fabricated flexible retina stimulator with 576 Pt/Au electrodes (left) and its opposite side (right). (d) The flexible retina stimulator after cutting vertical slits (left) for conformal contact to the retina, which has a spherical structure (right). (c-d) Reproduced with permission from ref. [34], © 2007, IOP Publishing Ltd.

metal-oxide semiconductor (CMOS) based scanning circuits have been applied to retinal stimulating electrode arrays [32-35]. Such arrays are partially flexible and can therefore fit onto the spherical eyeballs [36]. Such flexibility was realized by distributing rigid CMOS chips on flexible substrates (Fig. 3a) [37]. The fabricated device, which can be bent to a curvilinear surface with a radius of 1.7 mm (Fig. 3b, left), is also small enough to fit into various implantation sites on a rabbit's eye (Fig. 3b, right). For the electrical stimulation, platinum electrodes with a radius of 90 μm were patterned and connected to the CMOS-based scanning circuits. The pitches between electrodes were 240 (within the unit-chip) and 620 (between two adjacent unit chips) μm. These dimensions are comparable to or even smaller than those of the typical penetrating UEA, thus achieving high spatial resolution (Fig. 3b, left).

It has been suggested that arrays of more than 1000 electrodes can provide reasonable artificial vision to patients using implantable retina stimulators [34, 36]. By applying the aforementioned strategies of large-area partially flexible plastic substrates, Ohta *et al.* created a retina stimulator with 576 platinum/gold electrodes within a 8.8 mm × 9.1 mm array (Fig. 3c, left), with 64 microchips incorporated on the reverse side of the electrodes (Fig. 3c, right). A 1000-electrode stimulator can be achieved simply by using two sets of such 576-electrode stimulators [34], which provides enough stimulation points to achieve high-quality vision. Vertical slits are introduced in the stimulator (Fig. 3d, left) for enhanced flexibility (Fig. 3d, right). However, viable sites for implanting this hybrid-structured device are strictly limited owing to its large thickness, preventing implantation on uneven, corrugated surfaces such as the brain. Moreover, novel methods are required for attaching this device, which does not have adhesive properties, conformally to the target site.

Flexible passive electrode arrays

The mechanical mismatch at the electrode-to-neuron interfaces combined with local micro-motions of target organs may induce inflammatory reactions and progressive loss of electrode contact [38]. For long-term implantation with uncompromised signal quality, the flexibility of the electrode arrays is critical [39]. The development of microfabricated electrodes on flexible substrates such as silicone [40, 41], parylene [42], and polyimide [43, 44] has been reported. For instance, Yanai *et al.* reported that stimulation on the retinal surface of the human eye using a flexible silicone-based 16-electrode array can provide a simple visual experience to blind patients [41]. For higher resolution, a parylene-based 1024-electrode array (60 of them connected, Fig. 4a) was fabricated by the same group. It was implanted for 6 months onto the retina of canines with excellent biostability [42].

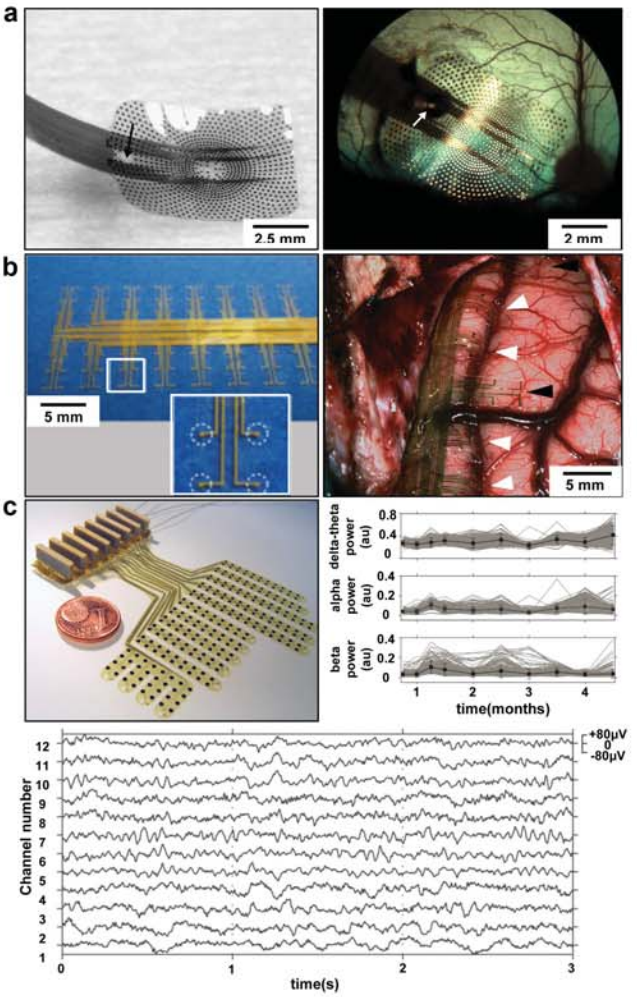

Fig. 4. Electrode arrays fabricated on the polymer substrates for flexibility: (a) Parylene based multielectrode arrays (60 of 1024 electrodes are connected) for retinal prosthesis (left). Fundus photograph of the multielectrode arrays attached on the right retina of a canine (right). Reproduced with permission from ref. [42], © 2008, Elsevier. (b) Flexible electrode arrays microfabricated on the parylene-C substrate (left). Dotted circles in the inset indicate the contact area. Photograph of flexible electrode arrays implanted on the left temporal lobe (right). White arrowheads denote probe branches implanted into the superior temporal sulcus (STS). Black arrowheads indicate branches on the superior temporal gyrus (STG). Reproduced with permission from ref. [45], © 2011, Matsuo T *et al.* (c) Fully assembled, polyimide based flexible electrode arrays (top left). The diameter of the coin is 16 mm. The development of the beta, alpha, and delta-theta band powers with implantation time (top right). The recorded local field potentials for 3 s from electrode arrays (bottom). Reproduced with permission from ref. [46], © 2009, IOP Publishing Ltd.

Matsuo *et al.* developed a parylene-C substrate (thickness: 20 μm) to fabricate a 128-channel flexible electrode array (Fig. 4b) for ECoG monitoring [45]. Using this array, they demonstrated ECoG measurements not only on the surface of the temporal gyrus but also on the intrasulcal cortices. The flexibility accomplished by using the polymer substrate

enables ECoG probes to be implanted properly even on valley-like structures. Rubehn *et al.* designed a 252-channel ECoG electrode array on a thin polyimide foil substrate (Fig. 4c, top left) [46]. They created a device large enough to cover the hemisphere of a macaque monkey's cortex. Using the flexible electrode array, they recorded local field potential signals as the monkey performed visual tasks (Fig. 4c, bottom). The long-term (4.5 months) evaluation showed that the implanted electrodes were still able to obtain good neural signals (Fig. 4c, top right). These studies on neural interfacing with flexible electrode arrays suggest possibilities for better biocompatibility and functional durability in chronic implantation than penetrating ones.

Excellent conformal coverage over the highly convoluted brain surface is required to firmly couple the electrodes and the brain cortex. However, conventional flexible electrode arrays fabricated with flexible substrates such as polyimide are too thick (~700 μm for clinical, >10 μm for research) [46, 47]. Fig. 5a and b show quantitative studies on the relationship between the device thickness and the conformal coverage over basic features that represent the brain curvature [48]. Fig. 5a shows the simplest case of a device with bending stiffness EI (product of the elastic modulus and the area moment of inertia), width b, thickness h, and length 2L, wrapped on a cylinder with radius R. Modeling and experiments shows that reducing the thickness improves wrapping capabilities (Fig. 5a, right). As an example, wrapping a layer around a cylindrical structure without adhesives is possible

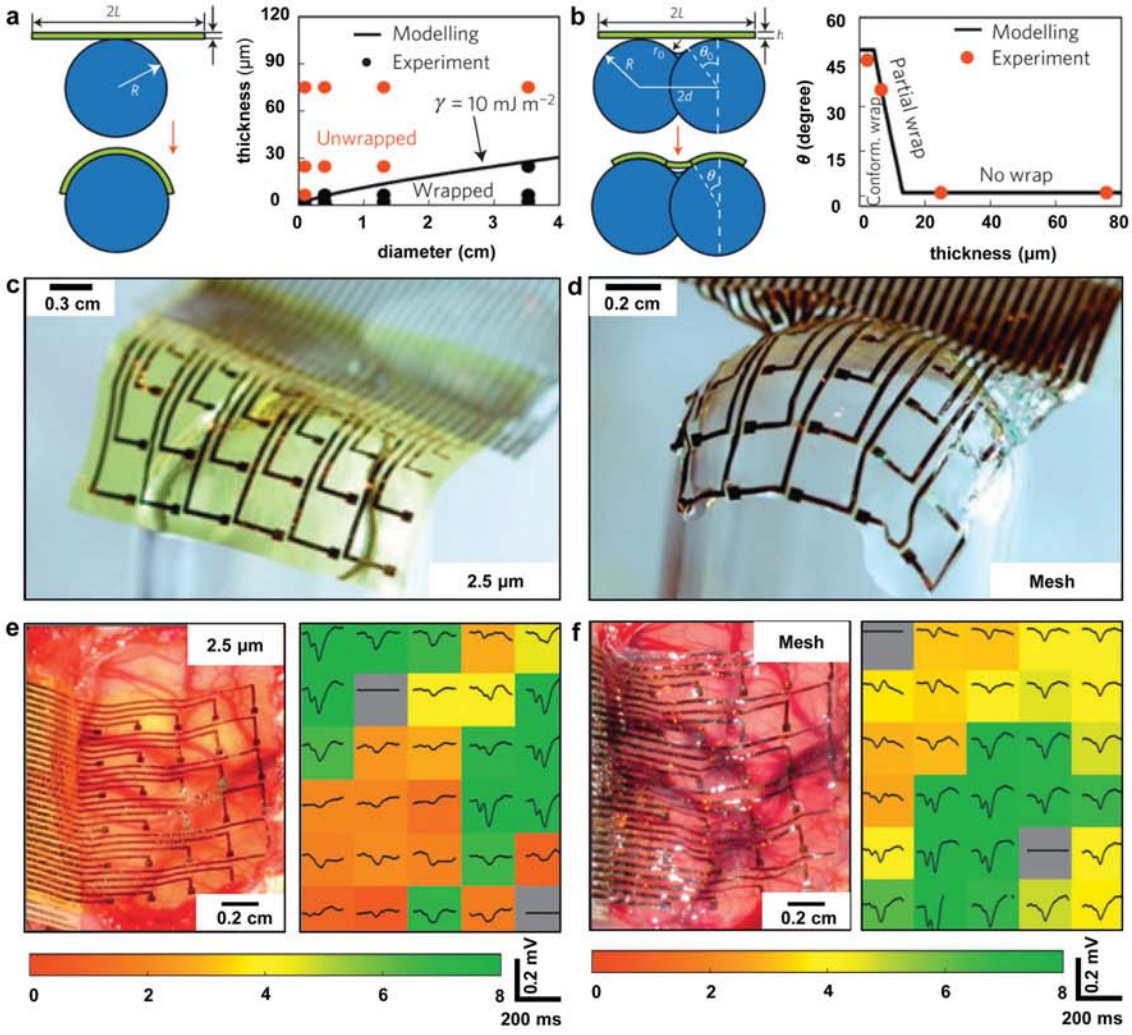

Fig. 5. Mesh-like structure for the conformal contact in neural interfacing: (a-b) Modelling (left) and simulations (right) for the wrapping characteristic on the simple cylinder substrate (a) and two overlapped cylinders (b). (c) Thin-film-type electrode array (2.5-μm thick) wrapped onto the glass hemisphere. (d) Electrode array with mesh structure wrapped onto the glass hemisphere. (e-f) Photographs of electrode arrays on a feline brain (left) and evoked responses from each electrode (right); 2.5-μm-thick sheet electrode array (e) and thick mesh electrode array (f). Color bars at the bottom denote root-mean-squared (RMS) amplitudes ratios for signal maps. Reproduced with permission from ref. [48], © 2010, Nature Publishing Group.

for R ~1 cm when h <~15 um. A pair of overlapped cylinders is used to simulate a simple model of a gyrus of the brain. Experimenting and modeling on a pair of overlapped cylinders shows consistent results with the simple cylinder model. For ultrathin (<10 μm) flexible electrode arrays, Kim *et al.* used bio-dissolvable silk fibroin as a temporary supporting substrate and fabricated a 2.5-μm-thick electrode array (Fig. 5c).

However, the substrate thickness is not the only important factor in achieving extremely conformal contact. The device geometry is also important [49]. Open mesh electrode arrays with 2.5-μm thickness achieve excellent conformal contact

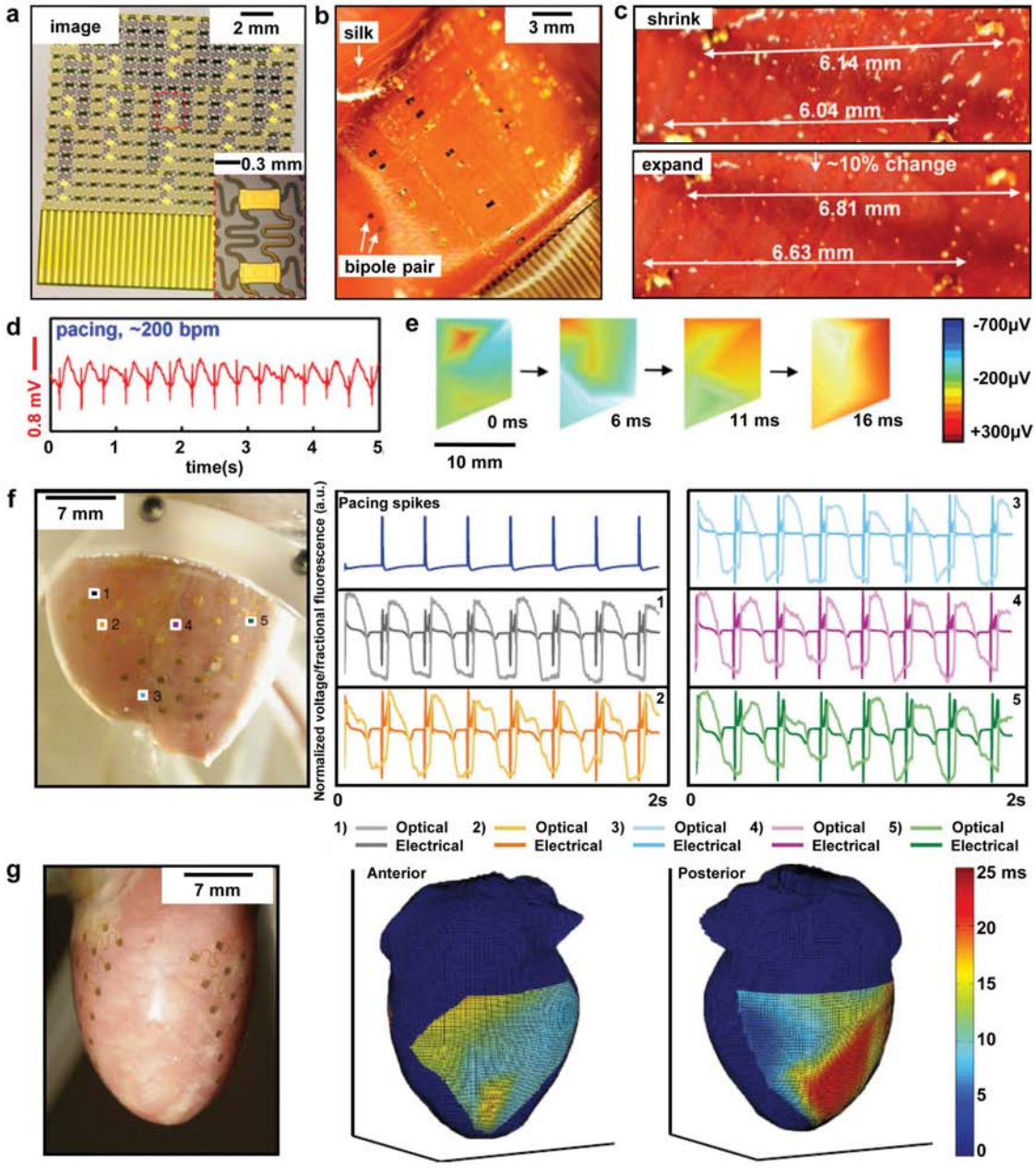

Fig. 6. Strategies for the conformal contact in cardiac interfacing: (a) Image of stretchable electrode web for cardiac mapping. (b) Mounted electrode web with the silk substrate on the cardiac surface. (c) Enlarged view of electrodes and interconnections moving synchronously with the cardiac deformation. (d) Recorded electrogram from the electrode web during rapid pacing session (~200 bpm). (e) Electrogram activation map patterns at several time intervals. The color bar indicates scale for potentials. (a-e) Reproduced with permission from ref. [57]. (f) Image of electrode arrays integrated with 3D membranes (left). Typical optical and electrical signals recorded simultaneously from the corresponding numbered electrode locations on a rabbit heart (center, right). (g) 3D maps of electrical signals acquired from both the anterior and posterior surfaces of the rabbit heart. (f, g) Reproduced with permission from ref. [58], © 2014, Nature Publishing Group.

over hemispherical substrates (Fig. 5d). A plain sheet design with the same thickness shows relatively poor contact (Fig. 5c). Improved conformal contact with ultrathin mesh structured electrodes enhances the signal-to-noise ratio (SNR) of the measured brain signals (Fig. 5e, f). The colored background represents the root mean square (RMS) amplitude ratios of channels (green = high, red = low). The 2.5-μm mesh structured electrodes exhibit better conformal contact and a higher mean RMS amplitude ratio than the sheet design electrode arrays.

As with the brain, electrophysiological mapping of the heart is also important for both basic research and clinical procedures [50, 51]. Existing approaches use various operation modes such as "sock"-type electrode arrays [52-54] and catheter-type delivery systems [55, 56]. These approaches utilize a passive metal wire mesh for electrophysiological mapping. Such mesh structures comprise wires that are millimeters in diameter. The large scale of individual electrodes causes interfacial mismatches between the electrode formats and the cardiac tissue. Because of the complex topographies and large, time-dynamic deformations, these mismatches may reduce the signal quality and induce inflammatory responses [57]. Therefore, high-quality, intimate contact between the epicardium and the electrodes is indispensable.

Owing to recent advancements in stretchable electronics, ultralow-modulus and stretchable electrode webs can overcome the abovementioned challenges [57]. Fig. 6a shows an epicardial flexible and stretchable electrode web for electrophysiological mapping. The patterns of sensors and actuators fabricated using microelectronic processing techniques are transferred onto a sacrificial silk film and mounted onto the surface of the heart (Fig. 6b). The physical properties—low effective stiffness and high degree of deformability—enable the device to couple with the underlying cardiac tissue (Fig. 6c). This contributes to the stability of the electrical signal under continuous deformation of the heart (Fig. 6d). Signals from the 17 electrodes on the anterior surface of the heart were converted into voltage color maps, and the activation pattern enabled an assessment of the directionality of wavefronts (Fig. 6e).

Recently, 3D integration of devices with an epicardial surface has been demonstrated [58]. A combined system with various sensors and electronic and optoelectronic components was built on the thin membrane molded using 3D printed heart model matching the shape of the heart. This system is capable of multifunctional, high-density epicardial mappings and stimulations. Fig. 6f shows optical and electrical signals captured from various locations on a Langendorff-perfused rabbit heart. Despite the deformations in the cardiac tissue, the optical and electrical signals captured using the 3D multifunctional integumentary membranes were not affected by movement artifacts owing to their induced movement being synchronous with the heart movement. Fig. 6g shows a 3D electrical signaling map derived from both the anterior and the posterior surfaces of the heart. These capabilities provide advanced methodological possibilities for basic and clinical cardiology.

Flexible active electrode arrays

There are two major limitations in signal acquisition using passive electrodes: (1) signals are transmitted through elongated wires before being amplified with an external device, resulting in high susceptibility to noise; (2) excessive wiring is required to achieve high spatial resolution. To overcome these limitations, active devices, especially field-effect transistors (FET) having good signal amplification capability [59-65], have been introduced for neural and cardiac activity monitoring. These transistors can significantly minimize system noise by providing on-site amplification [59, 60]. In this regard, Khodagholy *et al.* reported the first use of an organic transistor to record brain activity *in vivo* [60]. Fig. 7a shows the ECoG probe array using the organic electrochemical transistor (OECT) as an on-chip amplifier, laminated on a curvilinear surface. The OECT comprises poly-(3,4-ethylenedioxythiophene) doped with polystyrene sulfonate (PEDOT:PSS) as a transistor channel, and gold electrodes for source and drain contacts (Fig. 7a, right top inset). The array has 17 OECTs and 8 PEDOT:PSS surface electrodes for signal quality comparison, and it was placed on the somatosensory cortex (Fig. 7b). Time-frequency analysis was conducted using epileptiform activity data recorded by both OECT and surface electrodes (Fig. 7c). The results demonstrated that significantly better resolution was obtained from the OECT (SNR = 22.3 dB) than the PEDOT:PSS (SNR = 13.5 dB).

Active matrix addressing schemes developed for flat-panel displays have enabled the operation of hundreds of transistor arrays incorporated with hundreds of electrodes using only dozens of external leads. By applying this technology, mapping of neural activities and high-resolution electric signals captured on the surface of the brain can be achieved using only a small number of external wires [9]. Fig. 7d shows a 360-channel high-resolution multiplexed electrode array with excellent flexibility and a multilayer structure. Doped silicon nanoribbons were transferred onto the polymeric surface (polyimide) followed by the formation of horizontal and vertical metal interconnections insulated by polyimide layers (Fig. 7e, left). By placing a brittle silicon nanoribbon on the neutral mechanical plane where the bending-induced strain is essentially zero, the ribbons can remain intact during extreme bending [66]. Vertical holes that are horizontally offset by each other prevent the leakage

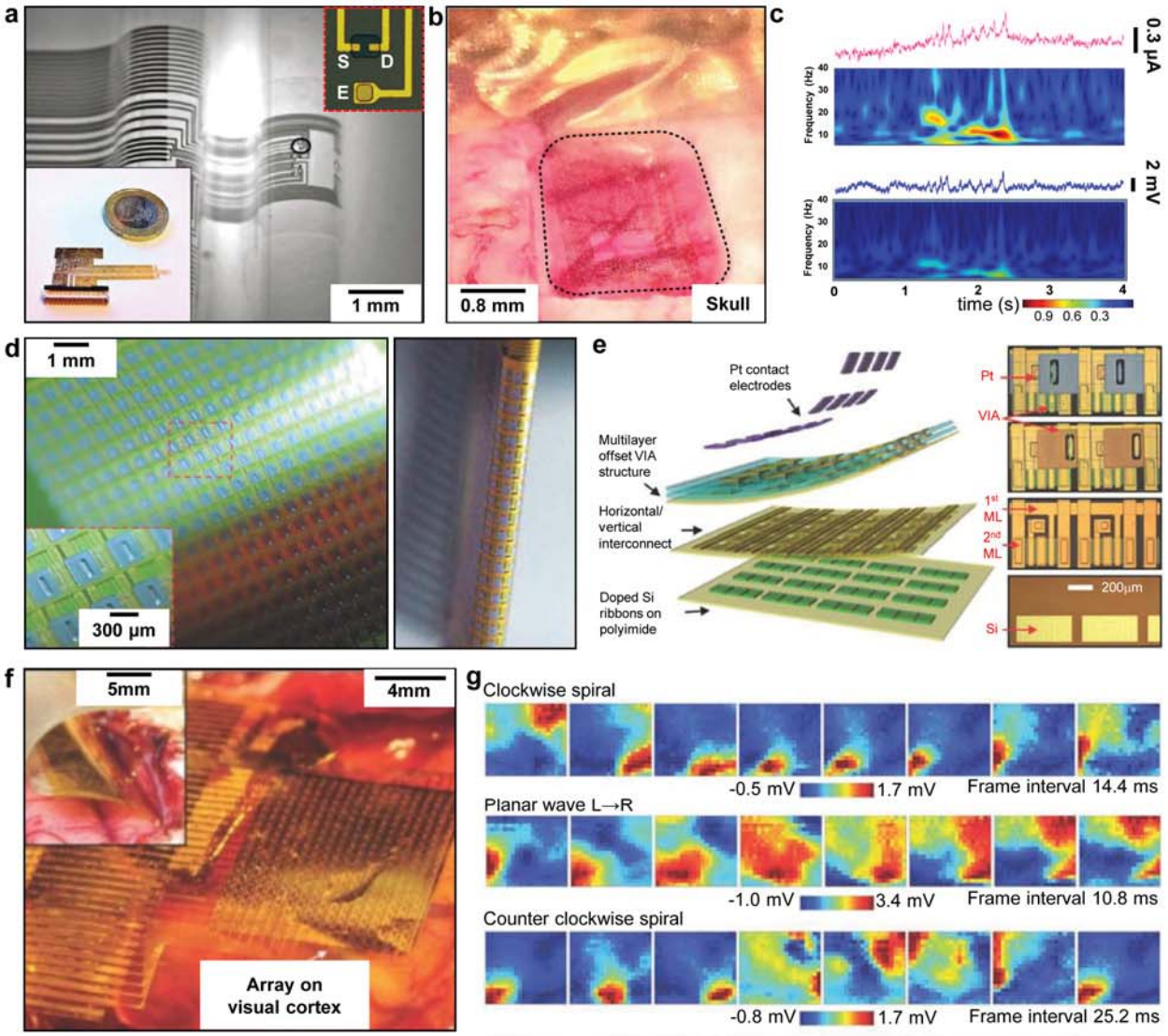

Fig. 7. Active neural electrode array: (a) A photograph of the active probe array incorporating organic electrochemical transistors (OECT) and surface electrodes (upper right inset) conforming onto a curvilinear surface. A size of whole electrode array with external connections is compared to the coin (left bottom inset). (b) A photograph of the electrode array placed on the somatosensory cortex. (c) Recordings from an OECT (top) and PEDOT:PSS surface electrode (bottom). Superior performances of the OECT are clearly shown in the SNR and resolution point of view. (a-c) Reproduced with permission from ref. [60], © 2013, Nature Publishing Group. (d) Flexible multiplexed electrode array having 360-channel (left). The inset shows the magnified view showing few cells. The flexible multiplexed electrode array showing its extreme flexibility (right). (e) Schematic exploded view of the flexible multiplexed electrode array (left) with corresponding pictures for each layer (right). (f) The flexible multiplexed electrode array is placed on the visual cortex. The inset shows its capability to be inserted in the interhemispheric fissure. (g) Various spatial-temporal ECoG voltage patterns during a short electrographic seizure. (d-g) Reproduced with permission from ref. [9], © 2011, Nature Publishing Group.

of the external conductive biofluid (Fig. 7e, right). Platinum electrodes were deposited and patterned on surface electrodes to reduce their impedance. The fabricated high-density electrode array was placed on the brain of a feline model (Fig. 7f). The array is flexible enough to be inserted into the interhemispheric fissure (Fig. 7f, inset). From the electrode array placed on the seizure evoked feline's neocortex, spatial-temporal ECoG voltage patterns from all 360 electrodes were successfully achieved and illustrated in a series of two-dimensional maps having specific time intervals (Fig. 7g). The recorded spatial patterns include right angle waves (data not shown), clockwise spirals, planar waves, and counter-clockwise spirals (Fig. 7g). Interestingly, the size of each pattern is approximately 1 cm × 1 cm, which is comparable

to the size of a typical clinical single electrode.

Similar strategies have been used for recording electrical activity from the epicardium for the diagnosis of cardiac arrhythmias. Conventional rigid electrode arrays that include only a few electrodes are typically used for this purpose [67]. Data are recorded from different spatial locations one at a time and analyzed post-experiment to produce a complete cardiac electrical activity map of the regions of interest; this process requires long time (more than tens of minutes) [68, 69]. Recently, the high-density multiplexed electrode array shown in Fig. 8a has been reported to map transient abnormal rhythms in real time [10]. Although this array contains 288 electrodes, only 36 output wires are required owing to the use of the active multiplexing method. Fig. 8b shows the electrode array placed on the porcine heart with conformal contacts. The array structure is only 25-μm thick, providing sufficient flexibility to maintain intimate contact with the rhythmically moving heart for stable signal recording. Fig. 8c shows sequential snapshots of the electrode array adhering to the porcine heart at various cardiac cycles, showing intimate contact despite energetic cardiac movement. In this manner, voltage data from all electrodes can be collected and plotted in a 2D spatial mapping image showing cardiac electric wave propagation (Fig. 8d). Such high temporal and spatial resolution monitoring of cardiac activity is essential for the diagnosis and therapy of cardiac arrhythmias.

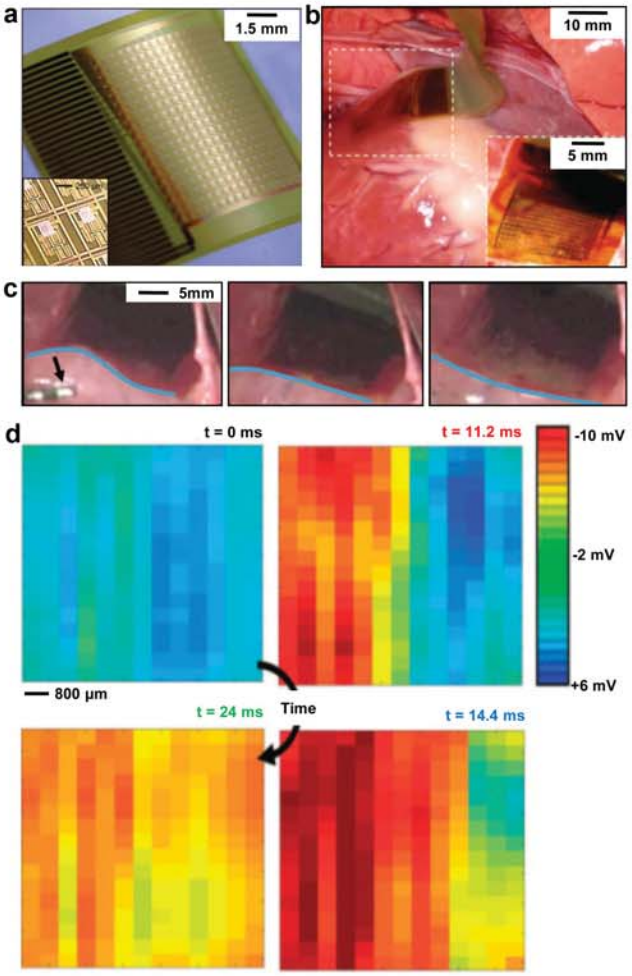

Fig. 8. Active cardiac electrode array: (a) A flexible multiplexed electrode array for cardiac mapping. (b) Photograph of the electrode array placed on the porcine heart. The inset shows the magnified view of the device. (c) Snap shots of the electrode array showing its conformability during the rhythmical movement of the heart. (d) Voltage patterns of the normal cardiac wave acquired from the electrode array at the different four points of the time. Reproduced with permission from ref. [10], © 2010, AAAS.

Magnetic resonance imaging (MRI) compatible electrode array

Integrating the data from the implanted electrode array and other brain imaging methodologies such as fMRI could provide new insights for cognitive neuroscience and clinical neurosurgery [70, 71]. However, conventional metal electrodes cause significant distortion of MRI images as well as RF-induced heat generation [72, 73]. In this regard, implantable electrode materials that are compatible with simultaneous MRI imaging have been studied. When different penetrating electrode materials (platinum-iridium, carbon, gold) were tested (Fig. 9a) [74], the paramagnetic platinum-iridium electrode was found to cause hyperintensity of the T2 signal (Fig. 9b, indicated by arrow), whereas carbon and gold electrodes caused minimal distortions (Fig. 9c, 9d).

Recently, Bonmassar *et al.* reported the MRI-compatible flexible electrode array, which is based on polymer thick-film organic substrates (PTFOS) (Fig. 9e) [75]. In this study, the MRI image quality was enhanced by using a reduced amount of metal and therefore the conductivity of the electrode/trace ink. MRI obtained in the presence of a PTFOS electrode array showed no signal distortion (Fig. 9h) when compared to the control experiment (MRI image without electrode, Fig. 9g), whereas a standard platinum electrode array caused significant distortion in the field map images (Fig. 9f). The PTFOS-based electrode array provides a promising example of MRI-compatible flexible electrode arrays. Further development of higher electrode density for high-spatial-resolution recording would be helpful for deducing clinically useful information using simultaneously acquired ECoG and brain image data.

CONCLUSION AND FUTURE WORK

Various strategies and techniques have been developed to realize high density flexible neural and cardiac electrode arrays, while conventional counterparts are rigid and sparse. In particular, studies have achieved the following: (1)

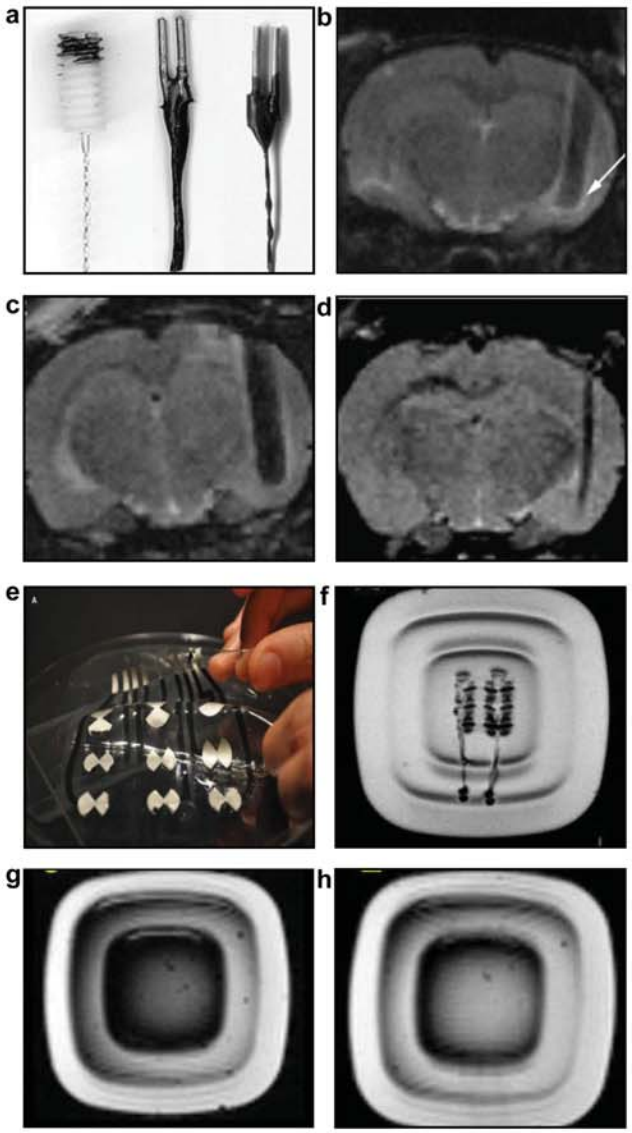

Fig. 9. MRI compatible electrodes: (a) Penetrating MRI compatible electrodes. From left to right: platinum-iridium bipolar; carbon fiber bipolar; and gold bipolar. (b-d) T2-weighted MRI images when the electrodes are implanted: axial image of platinum-iridium electrode with hyperintensity around the electrode indicated by the white arrow (b), carbon fiber electrode (c), and gold electrode (d). (a-d) Reproduced with permission from ref. [74], © 2006, Elsevier. (e) An image of polymer thick film organic substrate (PTFOS) flexible MRI compatible electrode array. Field map images of platinum electrode (f), control (g), and PTFOS electrode array (h). (e-h) Reproduced from ref. [75], © 2012, Bonmassar *et al*.

Electrode arrays with the thin and meshed structure have been constructed to enable intimate and conformal contacts between the electrodes and the constantly moving target organs. (2) Microfabrication technology has been applied to allow a dense arrangement of electrodes for high-spatial-resolution recording. (3) Multiplexing active devices have been applied to reduce the number of excessive external wires while maintaining the capability of addressing the sufficient number of electrodes within a small area for high-resolution mapping. (4) External amplifiers have been replaced with on-site devices to improve the SNR. (5) High-performance flexible silicon electronics have been introduced by placing brittle active silicon devices on the neutral mechanical plane where the bending induced strain converges to zero.

Recent advancements in flexible electronics have promoted the development of next-generation flexible, conformable, high-resolution electrode arrays that are concurrently compatible with other imaging techniques. Future works in this area should focus on the following issues: (1) ultra-large active matrix electrode arrays that can cover the entire surface of the heart or the brain; (2) dissolvable or degradable electrode arrays that can be removed without additional surgery; and (3) a self-sustainable integrated electrode array system that is self-powered by organ motion, with the wireless data transmitting capability. The current state-of-the-art technology allows only passive arrays to be incorporated to monitor the full surface of the heart. Combining large-area mapping with the high resolution enabled by multiplexing active arrays will not only improve the efficiency but also provide tremendous opportunities for the discovery of unknown clinical phenomena. The development of dissolvable electrode arrays would greatly simplify the removal of devices and lower the risk of complications [76]. Finally, the ultimate goal of implantable electrode arrays should be a fully integrated system with energy harvesting and wireless communication capabilities.

ACKNOWLEDGEMENTS

This work was supported by the Research Center Program of the Institute for Basic Science (IBS) of Korea. This work was also supported by a grant (2011-0031635) from the Center for Advanced Soft Electronics under the Global Frontier Research Program of the Ministry of Science, ICT and Future Planning, Korea, and by a grant from the Basic Science Research Program of the National Research Foundation of Korea (NRF), funded by the Ministry of Science, ICT and Future Planning (2012R1A1A1004925). N.L acknowledges the US NSF CMMI award under Grant No. 1301335. This work was also supported by the Seoul National University Research Grant.

CONFLICT OF INTEREST STATEMENTS

Kim J declares that he has no conflict of interest in relation to the work in this article. Lee M declares that he has no

conflict of interest in relation to the work in this article. Rhim JS declares that he has no conflict of interest in relation to the work in this article. Wang P declares that he has no conflict of interest in relation to the work in this article. Lu N declares that she has no conflict of interest in relation to the work in this article. Kim D-H declares that he has no conflict of interest in relation to the work in this article.

REFERENCES

[1] Jasper HH, Arfel-Capdeville G, Rasmussen T. Evaluation of EEG and cortical electrographic studies for prognosis of seizures following surgical excision of epileptogenic lesions. Epilepsia. 1961; 2(2):130-7.

[2] Crone NE. Functional mapping with ECoG spectral analysis. Adv Neurol. 2000; 84:343-51.

[3] Canolty RT, Edwards E, Dalal SS, Soltani M, Nagarajan SS, Kirsch HE, Berger MS, Barbaro NM, Knight RT. High gamma power is phase-locked to theta oscillations in human neocortex. Science. 2006; 313(5793):1626-8.

[4] McGonigal A, Bartolomei F, Régis J, Guye M, Gavaret M, Fonseca AT-D, Dufour H, Figarella-Branger D, Girard N, Péragut J-C, Chauvel P. Stereoelectroencephalography in presurgical assessment of MRI-negative epilepsy. Brain. 2007; 130(12):3169-83.

[5] Waldert S, Pistohl T, Braun C, Ball T, Aertsen A, Mehring C. A review on directional information in neural signals for brain-machine interfaces. J Physiol Paris. 2009; 103(3-5):244-54.

[6] Kato R, Lickfett L, Meininger G, Dickfeld T, Wu R, Juang G, Angkeow P, LaCorte J, Bluemke D, Berger R, Halperin HR, Calkins H. Pulmonary vein anatomy in patients undergoing catheter ablation of atrial fibrillation: lessons learned by use of magnetic resonance imaging. Circulation. 2003; 107(15):2004-10.

[7] Aziz JNY, Abdelhalim K, Shulyzki R, Genov R, Bardakjian BL, Derchansky M, Serletis D, Carlen PL. 256-channel neural recording and delta compression microsystem with 3D electrodes. IEEE J Solid-St Circ. 2009; 44(3):995-1005.

[8] Dewire J, Calkins H. State-of-the-art and emerging technologies for atrial fibrillation ablation. Nat Rev Cardiol. 2010; 7(3):129-38.

[9] Viventi J, Kim D-H, Vigeland L, Frechette ES, Blanco JA, Kim YS, Avrin AE, Tiruvadi VR, Hwang S-W, Vanleer AC, Wulsin DF, Davis K, Gelber CE, Palmer L, Van der Spiegel J, Wu J, Xiao J, Huang YG, Contreras D, Rogers JA, Litt B. Flexible, foldable, actively multiplexed, high-density electrode array for mapping brain activity in vivo. Nat Neurosci. 2011; 14(12):1599-605.

[10] Viventi J, Kim D-H, Moss JD, Kim Y-S, Blanco JA, Annetta N, Hicks A, Xiao J, Huang Y, Callans DJ, Rogers JA, Litt B. A conformal, bio-interfaced class of silicon electronics for mapping cardiac electrophysiology. Sci Transl Med. 2010; 2(24):24ra22.

[11] Normann RA. Technology Insight: future neuroprosthetic therapies for disorders of the nervous system. Nat Clin Pract Neurol. 2007; 3(8):444-52.

[12] Byun D, Cho SJ, Kim S. Fabrication of a flexible penetrating microelectrode array for use on curved surfaces of neural tissues. J Micromech Microeng. 2013; 23(12):125010.

[13] Moran D. Evolution of brain-computer interface: Action potentials, local field potentials and electrocorticograms. Curr Opin Neurobiol. 2010; 20(6):741-5.

[14] Gefen A, Margulies SS. Are in vivo and in situ brain tissues mechanically similar? J Biomech. 2004; 37(9):1339-52.

[15] Santhanam G, Linderman MD, Gilja V, Afshar A, Ryu SI, Meng TH, Shenoy KV. HermesB: A Continuous Neural Recording System for Freely Behaving Primates. IEEE T Biomed Eng. 2007; 54(11):2037-50.

[16] Branner A, Stein RB, Fernandez E, Aoyagi Y, Normann RA. Long-term stimulation and recording with a penetrating microelectrode array in cat sciatic nerve. IEEE T Biomed Eng. 2004; 51(1):146-57.

[17] Vince V, Thil M-A, Gérard A-C, Veraart C, Delbeke J, Colin IM. Cuff electrode implantation around the sciatic nerve is associated with an upregulation of TNF-α and TGF-β1. J Neuroimmunol. 2005; 159(1–2):75-86.

[18] Stieglitz T, Beutel H, Meyer J-U. A flexible, light-weight multichannel sieve electrode with integrated cables for interfacing regenerating peripheral nerves. Sensor Actuat A-Phys. 1997; 60(1–3):240-3.

[19] Takeuchi S, Suzuki T, Mabuchi K, Fujita H. 3D flexible multichannel neural probe array. J Micromech Microeng. 2004; 14(1):104-7.

[20] Kim S, Bhandari R, Klein M, Negi S, Rieth L, Tathireddy P, Toepper M, Oppermann H, Solzbacher F. Integrated wireless neural interface based on the Utah electrode array. Biomed Microdevices. 2009; 11(2):453-66.

[21] Ryu SI, Shenoy KV. Human cortical prostheses: lost in translation? Neurosurg Focus. 2009; 27(1):E5.

[22] Sugano H, Shimizu H, Sunaga S. Efficacy of intraoperative electrocorticography for assessing seizure outcomes in intractable epilepsy patients with temporal-lobe-mass lesions. Seizure. 2007; 16(2):120-7.

[23] Miller KJ, denNijs M, Shenoy P, Miller JW, Rao RPN, Ojemann JG. Real-time functional brain mapping using electrocorticography. NeuroImage. 2007; 37(2):504-7.

[24] Blakely T, Miller KJ, Zanos SP, Rao RPN, Ojemann JG. Robust, long-term control of an electrocorticographic brain-computer interface with fixed parameters. Neurosurg Focus. 2009; 27(1):E13.

[25] Leuthardt EC, Gaona C, Sharma M, Szrama N, Ronald J, Freudenberg Z, Solis J, Breshears J, Schalk G. Using the electrocorticographic speech network to control a brain-computer interface in humans. J Neural Eng. 2011; 8(3):036004.

[26] Graimann B, Huggins JE, Schlogl A, Levine SP, Pfurtscheller G. Detection of movement-related patterns in ongoing single-channel electrocorticogram. IEEE T Neural Syst Rehabil Eng. 2003; 11(3):276-81.

[27] Leuthardt EC, Miller KJ, Schalk G, Rao RPN, Ojemann JG. Electrocorticography-based brain computer Interface-the seattle experience. IEEE T Neural Syst Rehabil Eng. 2006; 14(2):194-8.

[28] Miller KJ, Schalk G, Fetz EE, den Nijs M, Ojemann JG, Rao RPN. Cortical activity during motor execution, motor imagery, and imagery-based online feedback. Proc Natl Acad Sci USA. 2010; 107(9):4430-5.

[29] Abel TJ, Rhone AE, Nourski KV, Granner MA, Oya H, Griffiths TD, Tranel DT, Kawasaki H, Howard MA. Mapping the temporal pole with a specialized electrode array: technique and preliminary results. Physiol Meas. 2014; 35(3):323-37.

[30] Chen C, Shin D, Watanabe H, Nakanishi Y, Kambara H, Yoshimura N, Nambu A, Isa T, Nishimura Y, Koike Y. Prediction of hand trajectory from electrocorticography signals in primary motor cortex. Plos One. 2013; 8(12):e83534.

[31] Rubehn B, Fries P, Stieglitz T. MEMS-Technology for large-scale, multichannel ECoG-electrode array manufacturing. Conf Proc IFMBE. 2008; 22:2413-6.

[32] Tokuda T, Pan YL, Uehara A, Kagawa K, Nunoshita M, Ohta J.

Flexible and extendible neural interface device based on cooperative multi-chip CMOS LSI architecture. Sensor Actuat A-Phys. 2005; 122(1):88-98.
[33] Tokuda T, Takeuchi Y, Noda T, Sasagawa K, Nishida K, Kitaguchi Y, Fujikado T, Tano Y, Ohta J, editors. Light-controlled retinal stimulation on rabbit using CMOS-based flexible multi-chip stimulator. Conf Proc IEEE Eng Med Biol Soc. 2009; 2009:646-9.
[34] Ohta J, Tokuda T, Kagawa K, Sugitani S, Taniyama M, Uehara A, Terasawa Y, Nakauchi K, Fujikado T, Tano Y. Laboratory investigation of microelectronics-based stimulators for large-scale suprachoroidal transretinal stimulation (STS). J Neural Eng. 2007; 4(1):S85-91.
[35] Tokuda T, Takeuchi Y, Sagawa Y, Noda T, Sasagawa K, Nishida K, Fujikado T, Ohta J. Development and in vivo Demonstration of CMOS-based multichip retinal stimulator with simultaneous multisite stimulation capability. IEEE T Biomed Circuits Sys. 2010; 4(6):445-53.
[36] Ohta J, Tokuda T, Sasagawa K, Noda T. Implantable CMOS biomedical devices. Sensors-Basel. 2009; 9(11):9073-93.
[37] Ohta J, Tokuda T, Kagawa K, Furumiya T, Uehara A, Terasawa Y, Ozawa M, Fujikado T, Tano Y. Silicon LSI-based smart stimulators for retinal prosthesis - a flexible and extendable microchip-based stimulator. IEEE Eng Med Biol Mag. 2006; 25(5):47-59.
[38] Borton D, Bonizzato M, Beauparlant J, DiGiovanna J, Moraud EM, Wenger N, Musienko P, Minev IR, Lacour SP, Millán JdR, Micera S, Courtine G. Corticospinal neuroprostheses to restore locomotion after spinal cord injury. Neurosci Res. 2014; 78:21-9.
[39] Yeager JD, Phillips DJ, Rector DM, Bahr DF. Characterization of flexible ECoG electrode arrays for chronic recording in awake rats. J Neurosci Methods. 2008; 173(2):279-85.
[40] Liang G, Guvanasen GS, Xi L, Tuthill C, Nichols TR, DeWeerth SP. A PDMS-based integrated stretchable microelectrode array (isMEA) for neural and muscular surface interfacing. IEEE T Biomed Circuits Sys. 2013; 7(1):1-10.
[41] Yanai D, Weiland JD, Mahadevappa M, Greenberg RJ, Fine I, Humayun MS. Visual performance using a retinal prosthesis in three subjects with retinitis pigmentosa. Am J Ophthalmol. 2007;143(5):820-7.
[42] Rodger DC, Fong AJ, Li W, Ameri H, Ahuja AK, Gutierrez C, Lavrov I, Zhong H, Menon PR, Meng E, Burdick JW, Roy RR, Edgerton VR, Weiland JD, Humayun MS, Tai Y-C. Flexible parylene-based multielectrode array technology for high-density neural stimulation and recording. Sensor Actuat B-Chem. 2008; 132(2):449-60.
[43] Stieglitz T, Beutel H, Schuettler M, Meyer J-U. Micromachined, Polyimide-based devices for flexible neural interfaces. Biomed Microdevices. 2000; 2(4):283-94.
[44] Sauter-Starace F, Bibari O, Berger F, Caillat P, Benabid AL. ECoG recordings of a non-human primate using carbon nanotubes electrodes on a flexible polyimide implant. Conf Proc IEEE Eng Med Biol Soc. 2009; 2009:112-5.
[45] Matsuo T, Kawasaki K, Osada T, Sawahata H, Suzuki T, Shibata M, Miyakawa N, Nakahara K, Iijima A, Sato N, Kawai K, Saito N, Hasegawa I. Intrasulcal electrocorticography in macaque monkeys with minimally invasive neurosurgical protocols. Front Syst Neurosci. 2011; 5:34.
[46] Rubehn B, Bosman C, Oostenveld R, Fries P, Stieglitz T. A MEMS-based flexible multichannel ECoG-electrode array. J Neural Eng. 2009; 6(3):036003.
[47] Hollenberg BA, Richards CD, Richards R, Bahr DF, Rector DM. A MEMS fabricated flexible electrode array for recording surface field potentials. J Neurosci Methods. 2006; 153(1):147-53.
[48] Kim D-H, Viventi J, Amsden JJ, Xiao J, Vigeland L, Kim Y-S, Blanco JA, Panilaitis B, Frechette ES, Contreras D, Kaplan DL, Omenetto FG, Huang Y, Hwang K-C, Zakin MR, Litt B, Rogers JA. Dissolvable films of silk fibroin for ultrathin conformal bio-integrated electronics. Nat Mater. 2010; 9(6):511-7.
[49] Toda H, Suzuki T, Sawahata H, Majima K, Kamitani Y, Hasegawa I. Simultaneous recording of ECoG and intracortical neuronal activity using a flexible multichannel electrode-mesh in visual cortex. Neuroimage. 2011; 54(1):203-12.
[50] Dhein S, Muller A, Klaus W. Prearrhythmia: changes preceding arrhythmia, new aspects by epicardial mapping. Basic Res Cardiol. 1990; 85(3):285-96.
[51] Gepstein L, Hayam G, Ben-Haim SA. A novel method for nonfluoroscopic catheter-based electroanatomical mapping of the heart. In vitro and in vivo accuracy results. Circulation. 1997; 95(6):1611-22.
[52] Faris OP, Evans FJ, Ennis DB, Helm PA, Taylor JL, Chesnick AS, Guttman MA, Ozturk C, McVeigh ER. Novel technique for cardiac electromechanical mapping with magnetic resonance imaging tagging and an epicardial electrode sock. Ann Biomed Eng. 2003; 31(4):430-40.
[53] Harrison L, Ideker RE, Smith WM, Klein GJ, Kasell J, Wallace AG, Gallagher JJ. The sock electrode array: a tool for determining global epicardial activation during unstable arrhythmias. Pacing Clin Electrophysiol. 1980; 3(5):531-40.
[54] Sutherland DR, Ni Q, MacLeod RS, Lux RL, Punske BB. Experimental measures of ventricular activation and synchrony. Pacing Clin Electrophysiol. 2008; 31(12):1560-70.
[55] Hindricks G, Kottkamp H. Simultaneous noncontact mapping of left atrium in patients with paroxysmal atrial fibrillation. Circulation. 2001; 104(3):297-303.
[56] Ouyang F, Ernst S, Chun J, Bansch D, Li Y, Schaumann A, Mavrakis H, Liu X, Deger FT, Schmidt B, Xue Y, Cao J, Hennig D, Huang H, Kuck KH, Antz M. Electrophysiological findings during ablation of persistent atrial fibrillation with electroanatomic mapping and double Lasso catheter technique. Circulation. 2005; 112(20):3038-48.
[57] Kim D-H, Ghaffari R, Lu N, Wang S, Lee SP, Keum H, D'Angelo R, Klinker L, Su Y, Lu C, Kim Y-S, Ameen A, Li Y, Zhang Y, de Graff B, Hsu YY, Liu Z, Ruskin J, Xu L, Lu C, Omenetto FG, Huang Y, Mansour M, Slepian MJ, Rogers JA. Electronic sensor and actuator webs for large-area complex geometry cardiac mapping and therapy. Proc Natl Acad Sci USA. 2012; 109(49):19910-5.
[58] Xu L, Gutbrod SR, Bonifas AP, Su Y, Sulkin MS, Lu N, Chung HJ, Jang KI, Liu Z, Ying M, Lu C, Webb RC, Kim JS, Laughner JI, Cheng H, Liu Y, Ameen A, Jeong JW, Kim GT, Huang Y, Efimov IR, Rogers JA. 3D multifunctional integumentary membranes for spatiotemporal cardiac measurements and stimulation across the entire epicardium. Nat Commun. 2014; 5:3329.
[59] Olsson RH, Gulari MN, Wise KD. Silicon neural recording arrays with on-chip electronics for in-vivo data acquisition. Conf Proc IEEE-EMB Spec Top Conf Microtech Med Biol. 2002; 237-40.
[60] Khodagholy D, Doublet T, Quilichini P, Gurfinkel M, Leleux P, Ghestem A, Ismailova E, Herve T, Sanaur S, Bernard C, Malliaras GG. In vivo recordings of brain activity using organic transistors. Nat Commun. 2013; 4:1575.
[61] Han S-J, Jenkins KA, Valdes Garcia A, Franklin AD, Bol AA, Haensch W. High-frequency graphene voltage amplifier. Nano Lett. 2011; 11(9):3690-3.
[62] Andersson MA, Habibpour O, Vukusic J, Stake J. 10 dB small-signal graphene FET amplifier. Electron Lett. 2012; 48(14):861-3.
[63] Yang X, Liu G, Balandin AA, Mohanram K. Triple-mode single-transistor graphene amplifier and its applications. ACS Nano. 2010; 4(10):5532-8.

[64] Klauk H, Zschieschang U, Halik M. Low-voltage organic thin-film transistors with large transconductance. J Appl Phys. 2007; 102(7):074514.
[65] Hutzler M, Fromherz P. Silicon chip with capacitors and transistors for interfacing organotypic brain slice of rat hippocampus. Eur J Neurosci. 2004; 19(8):2231-8.
[66] Kim D-H, Ahn J-H, Choi WM, Kim H-S, Kim T-H, Song J, Huang YY, Liu Z, Lu C, Rogers JA. Stretchable and foldable silicon integrated circuits. Science. 2008; 320(5875):507-11.
[67] Friedman PA. Novel mapping techniques for cardiac electrophysiology. Heart. 2002; 87(6):575-82.
[68] Aliot EM, Stevenson WG, Almendral-Garrote JM, Bogun F, Calkins CH, Delacretaz E, Bella PD, Hindricks G, Jaïs P, Josephson ME, Kautzner J, Kay GN, Kuck K-H, Lerman BB, Marchlinski F, Reddy V, Schalij M-J, Schilling R, Soejima K, Wilber D. EHRA/HRS expert consensus on catheter ablation of ventricular arrhythmias: developed in a partnership with the European Heart Rhythm Association (EHRA), a Registered Branch of the European Society of Cardiology (ESC), and the Heart Rhythm Society (HRS); in collaboration with the American College of Cardiology (ACC) and the American Heart Association (AHA). Europace. 2009; 11(6):771-817.
[69] Scherlag BJ, Lau SH, Helfant RH, Berkowitz WD, Stein E, Damato AN. Catheter technique for recording his bundle activity in man. Circulation. 1969; 39(1):13-8.
[70] Laufs H, Daunizeau J, Carmichael DW, Kleinschmidt A. Recent advances in recording electrophysiological data simultaneously with magnetic resonance imaging. Neuroimage. 2008; 40(2):515-28.
[71] Gotman J, Kobayashi E, Bagshaw AP, Benar CG, Dubeau F. Combining EEG and fMRI: a multimodal tool for epilepsy research. J Magn Reson Imaging. 2006; 23(6):906-20.
[72] Bhavaraju NC, Nagaraddi V, Chetlapalli SR, Osorio I. Electrical and thermal behavior of non-ferrous noble metal electrodes exposed to MRI fields. Magn Reson Imaging. 2002; 20(4):351-7.
[73] Davis LM, Spencer DD, Spencer SS, Bronen RA. MR imaging of implanted depth and subdural electrodes: is it safe? Epilepsy Res. 1999; 35(2):95-8.
[74] Jupp B, Williams JP, Tesiram YA, Vosmansky M, O'Brien TJ. MRI compatible electrodes for the induction of amygdala kindling in rats. J Neurosci Methods. 2006; 155(1):72-6.
[75] Bonmassar G, Fujimoto K, Golby AJ. PTFOS: Flexible and Absorbable Intracranial Electrodes for Magnetic Resonance Imaging. Plos One. 2012; 7(9):e41187.
[76] Hwang S-W, Tao H, Kim D-H, Cheng H, Song J-K, Rill E, Brenckle MA, Panilaitis B, Won SM, Kim Y-S, Song Y-M, Yu K-J, Ameen A, Li R, Su Y, Yang M, Kaplan DL, Zakin MR, Slepian MJ, Huang Y, Omenetto FG, Rogers JA. A physically transient form of silicon electronics. Science. 2012; 337(6102): 1640-4.